

*Garaga M.N. et al., Local Environments around Heteroatoms in Layered Borosilicates,
Supporting Information*

Local Environments of Boron Heteroatoms in Non- Crystalline Layered Borosilicates

Mounesha N. Garaga,^a Ming-Feng Hsieh,^b Zalfa Nour,^a

Michael Deschamps,^a Dominique Massiot,^a Bradley F. Chmelka,^b Sylvian Cadars^{a,c,}*

^a CNRS, CEMHTI UPR3079, Univ. Orléans, F-45071 Orléans, France

^b Department of Chemical Engineering, University of California, Santa Barbara, California

93106, U.S.A

^c present address: Institut des Matériaux Jean Rouxel (IMN), Université de Nantes, CNRS, 2 rue de la Houssinière, BP32229, 44322 Nantes cedex 3, France

* To whom correspondence should be addressed: E-mail: sylvian.cadars@cnrs-imn.fr

Dr. Sylvian Cadars

Institut des Matériaux Jean Rouxel (IMN), UMR6502, Université de Nantes, CNRS,

2 rue de la Houssinière, BP32229, 44322 Nantes cedex 3, France

E-mail : sylvian.cadars@cnrs-imn.fr

Supporting information

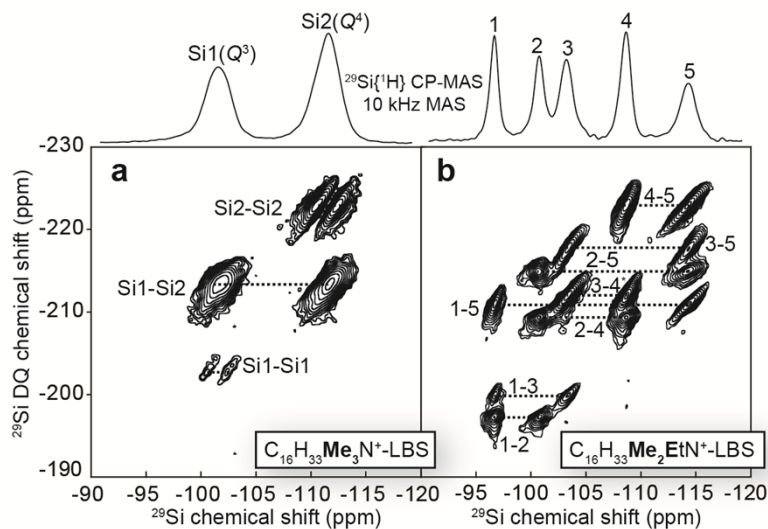


Figure S1. Solid-state NMR ^{29}Si refocused INADEQUATE spectra probing ^{29}Si -O- ^{29}Si linkages in ^{29}Si -enriched (a) $\text{C}_{16}\text{H}_{33}\text{N}^+\text{Me}_3\text{-}$ and (b) $\text{C}_{16}\text{H}_{33}\text{N}^+\text{Me}_2\text{Et-}$ directed layered borosilicates ($\text{Si}/\text{B} = 140$ and 52 , respectively), collected on a BRUKER AVANCE I spectrometer equipped with a magnetic field of 7.0 T (^1H and ^{29}Si Larmor frequencies of 300 and 59.63 MHz , respectively). The sample was spun at a MAS frequency of 10 kHz with a 4 mm double resonance probehead. A half-echo delay of 6 ms and a cross-polarization (CP) contact time of 7 ms were used for both materials. The spectra were accumulated over 128 and 96 transients for each of 160 and 184 increments in the indirect dimension, respectively. Heteronuclear ^1H decoupling (SPINAL64) of 60 kHz was applied during the entire pulse sequence.

Table S1. Perturbation range induced by the B atoms.

Materials	Si/B	Perturbation range (Å)	Number of Si neighbors affected ^a	% of ²⁹Si signal affected ^b
C ₁₆ H ₃₃ Me ₃ N ⁺ -directed layered borosilicate	140	4	3.5	2.5
		5	10	7
		6	13.5	10
		7	16.5	12
		8	28	20
C ₁₆ H ₃₃ Me ₂ EtN ⁺ -directed layered borosilicate	52	4	3.6	7
		5	9.2	18
		6	14.2	27
		7	19.0	37
		8	28.8	55

^a The number of Si sites affected by the presence of a B atom nearby were calculated as follows. Considering a given silicate framework model of the material considered (taken from refs.1, 2 for the C₁₆H₃₃Me₃N⁺ and C₁₆H₃₃Me₂EtN⁺ - directed materials, respectively), we substituted one Si site by a B atom and counted the number of Si atoms located within the chosen perturbation range. This task was repeated for B substituting each one of the (two or five, respectively) inequivalent T sites. The value given here is the average of the number of Si sites counted in all cases.

^b the fraction of ²⁹Si signal affected is calculated as the number of Si affected divided by the Si/B ratio.

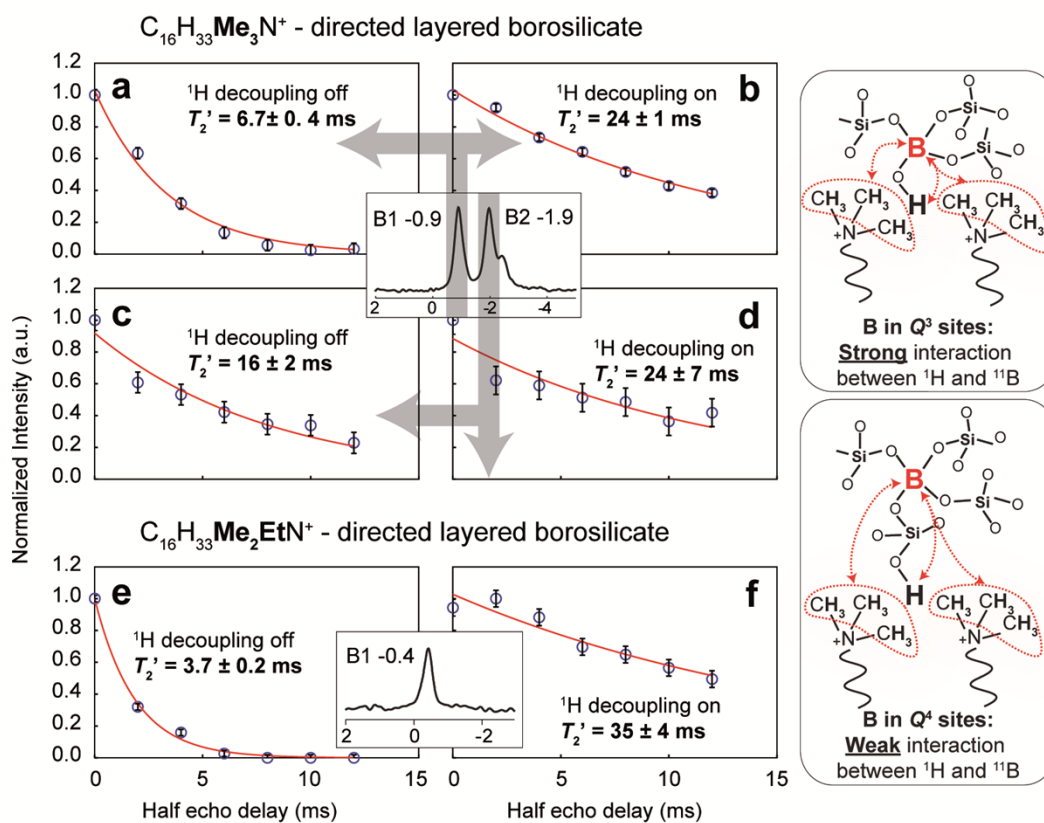
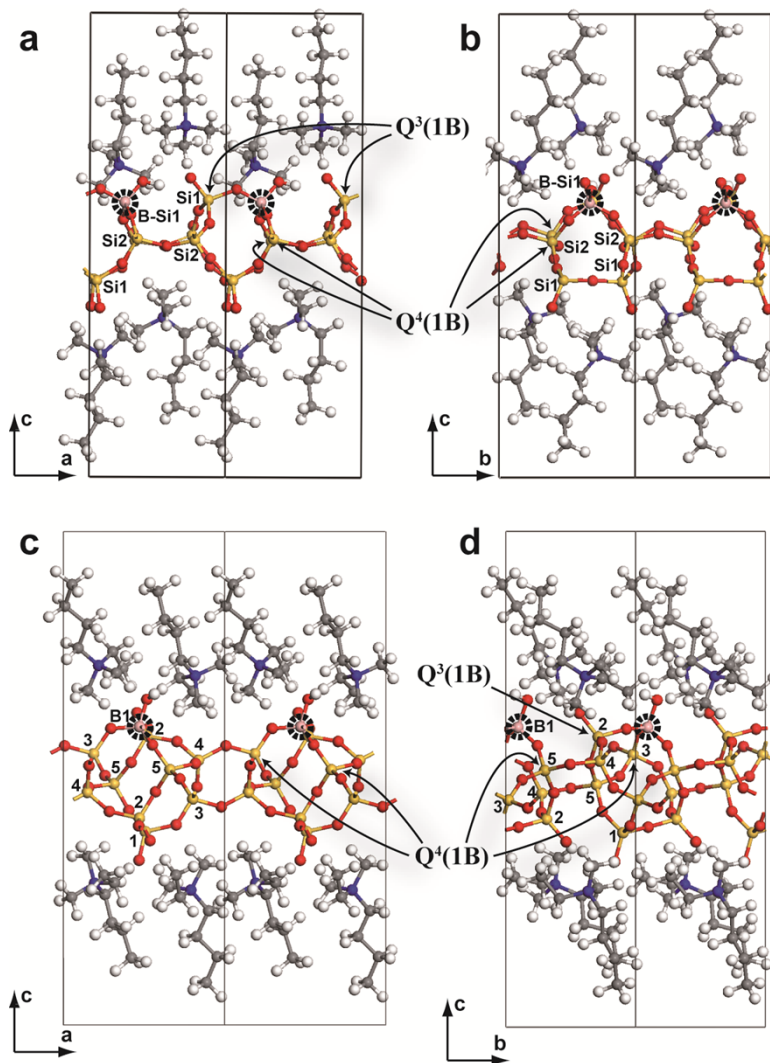


Figure S2. Transverse ^{11}B dephasing time (T_2') measurements conducted (a, c, e) without and (b, d, f) with heteronuclear 1H decoupling on (a-d) $C_{16}H_{33}Me_3N^+$ - and (e, f) $C_{16}H_{33}Me_2EtN^+$ -directed layered borosilicates to make distinction between Q^3 and Q^4 ^{11}B environments. While Q^3 sites dephase much more rapidly without than with heteronuclear 1H decoupling due to the closer proximity of 1H moieties, Q^4 sites are not strongly affected since their couplings to the protons are weaker.

Description of DFT calculations using surfactant-mimicking molecules. In addition to the computational results based on the approximation where the charge-compensating alkylammonium surfactants are simply omitted, another approach was also conducted, in which surfactant-mimicking molecules were incorporated explicitly. Specifically, short alkyl-chain $\text{CH}_3\text{-(CH}_2\text{)}_3\text{-N}^+\text{Me}_3$ or $\text{CH}_3\text{-(CH}_2\text{)}_3\text{-N}^+\text{Me}_2\text{Et}$ molecules were included in the inter-layer space of all reference layered silicate structure models to streamline computations while hopefully describing the organic-inorganic interactions at the interface. A series of geometry optimizations were then conducted on model structures, in which one of the Si sites was manually replaced by one B atom. Several models containing different amounts of these surfactant-mimicking molecules were used for both materials. In the case where the number of surfactant molecule is less than the negative charge presented in a specific structure, protons are added to form B(or Si)-O-H \cdots O-Si species. Examples of B atoms in Q^3 Si sites in the $\text{C}_4\text{H}_9\text{N}^+\text{Me}_3$ and $\text{C}_4\text{H}_9\text{N}^+\text{Me}_2\text{Et}$ -directed borosilicates are shown in Figure S2 (a, b) and (c, d), respectively. Other examples of compositions for model structures of the material with $\text{-N}^+\text{Me}_3$ headgroups are listed in Table S3.



addition of a proton on the boron in Q^3 site. The black lines delimit the unit cell, with two adjacent cells shown in each case.

While model structures built with the approach described above were expected to describe the local Si structures near framework B species, calculated ^{29}Si chemical shifts are not consistent with the NMR analyses of $\text{C}_{16}\text{H}_{33}\text{N}^+\text{Me}_3^-$ and $\text{C}_{16}\text{H}_{33}\text{N}^+\text{Me}_2\text{Et}$ - directed layered borosilicate materials. This is illustrated in Figure S3 for the $\text{C}_4\text{H}_9\text{N}^+\text{Me}_2\text{Et}$ - directed layered borosilicate models, for which broad distributions of calculated ^{29}Si chemical shifts are obtained, which are not well correlated with experimental results, and probably result from the frozen state of the surfactant-mimicking molecules. Similar observations were made for the $\text{C}_4\text{H}_9\text{N}^+\text{Me}_3^-$ - directed models (data not shown), confirming that the surfactant dynamics crucially impact the ^{29}Si NMR signatures (as already discussed from variable-temperature experiments on the reference $\text{C}_{16}\text{H}_{33}\text{N}^+\text{Me}_2\text{Et}$ - directed layered silicate material³). Although the ^{11}B chemical shifts calculated via this approach (see Tables S2 and S3) turn out to be less affected by this issue than ^{29}Si chemical shifts, a different modeling strategy was adopted for these systems.

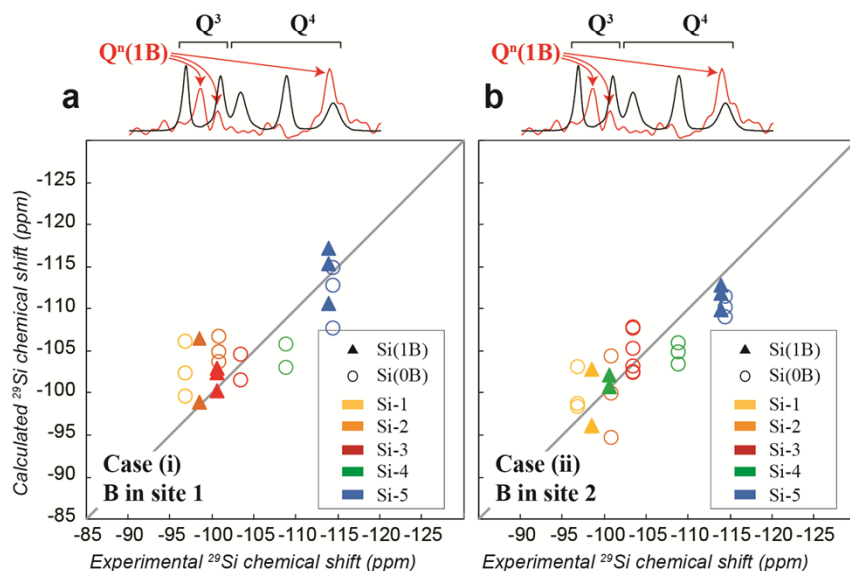


Figure S4. Comparisons of experimental ^{29}Si chemical shifts and isotropic chemical shifts calculated by DFT for a series of $\text{C}_4\text{H}_9\text{Me}_2\text{EtN}^+$ - directed borosilicate models of composition $(\text{BSi}_9\text{O}_{11})^{5-} \cdot 4(\text{C}_4\text{H}_9\text{N}^+\text{Me}_2\text{Et})$. Shown in black above the plots are the $^{29}\text{Si}\{^1\text{H}\}$ CP-MAS collected for the corresponding materials, and in red are projections extracted from 2D $^{11}\text{B}\{^{29}\text{Si}\}$ correlation experiments revealing $Q^n(1\text{B})$ ^{29}Si environments. Open “o” symbols in (a), (b) correspond to Si atoms that are not connected to a B atom, and whose experimental shifts should correspond (in first approximation) to the dominant ^{29}Si peaks observed experimentally (and identical to pure-silicate materials). Plots (a) and (b) correspond to two distinct situations, with B incorporated either (a) in Q^3 crystallographic site 1 or (b) in Q^3 crystallographic site 2, with the resulting calculated $Q^n(1\text{B})$ ^{29}Si shifts shown as filled “▲” symbols. Studied models are based on the three candidate structures of the $\text{C}_{16}\text{H}_{33}\text{Me}_2\text{EtN}^+$ - directed layered silicate material (see ref. 4).

Table S2. ^{11}B chemical shift values calculated with DFT for the model structures of the $\text{C}_{16}\text{H}_{33}\text{N}^+\text{Me}_2\text{Et}$ - layered borosilicate material with $\text{C}_4\text{H}_9\text{N}^+\text{Me}_2\text{Et}$ surfactant-mimicking molecules.

Material Model	B/Si substitution site	Range of calculated isotropic ^{11}B chemical shifts (ppm) ^a	Experimental ^{11}B shift (ppm) ^b
$\text{C}_4\text{H}_9\text{Me}_2\text{EtN}^+$ - layered borosilicate	Si1(Q^3)	-1.1 to -0.8	-0.4
	Si2(Q^3)	-1.3 to 0.4	
	Si3(Q^4)	-1.9 to -1.6	
	Si4(Q^4)	-3.5 to -2.1	
	Si5(Q^4)	-3.9 to -2.2	

^a The range of values given here includes calculations conducted on models built from different reference silicate structures (candidate structures #2, 3, or 4 in ref. 2), with compositions $(\text{BSi}_9\text{O}_{11})^{5-} \cdot 4(\text{C}_4\text{H}_9\text{N}^+\text{Me}_2\text{Et})$ in a $1 \times 1 \times 1$ cell.

^b Position of ^{11}B peak at 17.6 T. This value should be close to the actual chemical shift value because the quadrupolar interaction, and thus the corresponding contribution to the isotropic shift of these $^{11}\text{B}^{(\text{IV})}$ is small (< 1 MHz, as predicted from DFT calculations).

Table S3. ^{11}B chemical shift values calculated with DFT for the model structures of the $\text{C}_{16}\text{H}_{33}\text{N}^+\text{Me}_3$ - layered borosilicate material with different amounts of $\text{C}_4\text{H}_9\text{N}^+\text{Me}_3$ surfactant-mimicking molecules.

Model composition and charge	B/Si substitution site	New framework connectivity	BOH/SiOH groups	Supercell size	Calculated $\delta_{\text{iso}}(^{11}\text{B})$ (ppm)	Experimental ^{11}B shift (ppm) ^a
$(\text{BSi}_7\text{O}_{18})^{5-} \cdot 5(\text{C}_4\text{H}_9\text{N}^+\text{Me}_3)$	Si1(Q^3) as BO $^-$	None		1x1x1	-0.7	-0.9
$(\text{BSi}_{15}\text{O}_{36})^{9-} \cdot 9(\text{C}_4\text{H}_9\text{N}^+\text{Me}_3)$	Si1(Q^3) as BO $^-$	None		1x2x1	-0.1	-0.9
$(\text{BSi}_7\text{O}_{18}\text{H})^{4-} \cdot 4(\text{C}_4\text{H}_9\text{N}^+\text{Me}_3)$	Si1(Q^3) as BOH	None	1 BOH	1x1x1	-0.6	-0.9
$(\text{BSi}_{15}\text{O}_{36}\text{H}_8)^- \cdot (\text{C}_4\text{H}_9\text{N}^+\text{Me}_3)$	Si1(Q^3) as BOH	None	1 BOH / 7 SiOH	1x2x1	-1.2	-0.9
$(\text{BSi}_7\text{O}_{18})^{5-} \cdot 5(\text{C}_4\text{H}_9\text{N}^+\text{Me}_3)$	Si2(Q^4)	None		1x1x1	-1.9	-2.5
$(\text{BSi}_{15}\text{O}_{36})^{9-} \cdot 9(\text{C}_4\text{H}_9\text{N}^+\text{Me}_3)$	Si2(Q^4)	None		1x2x1	-1.7	-2.5
$(\text{BSi}_7\text{O}_{18}\text{H})^{4-} \cdot 4(\text{C}_4\text{H}_9\text{N}^+\text{Me}_3)$	Si2(Q^4)	None	1 SiOH	1x1x1	-2.7	-2.5
$(\text{BSi}_{15}\text{O}_{36}\text{H}_8)^- \cdot (\text{C}_4\text{H}_9\text{N}^+\text{Me}_3)$	Si2(Q^4)	None		1x2x1	-2.4	-2.5
Models with additional Si-O-Si connectivities						
$(\text{BSi}_{23}\text{O}_{53}\text{H})^{10-} \cdot 10(\text{C}_4\text{H}_9\text{N}^+\text{Me}_3)$	Si1(Q^3)	1 Si-O-Si	1 BOH	1x3x1	0.1	-0.9
$(\text{BSi}_{23}\text{O}_{53}\text{H}_{10})^- \cdot (\text{C}_4\text{H}_9\text{N}^+\text{Me}_3)$	Si1(Q^3)	1 Si-O-Si	1 BOH / 9 SiOH	1x3x1	-0.4	-0.9
$(\text{BSi}_{47}\text{O}_{107}\text{H}_{22})^- \cdot (\text{C}_4\text{H}_9\text{N}^+\text{Me}_3)$	Si1(Q^3)	1 Si-O-Si	1 BOH / 21 SiOH	2x3x1	0.1	-0.9
$(\text{BSi}_{31}\text{O}_{71}\text{H})^{14-} \cdot 14(\text{C}_4\text{H}_9\text{N}^+\text{Me}_3)$	Si2(Q^4)	1 Si-O-Si	1 SiOH	2x2x1	-2.3, -3.3 ^b	-2.5
$(\text{BSi}_{31}\text{O}_{71})^{15-} \cdot 15(\text{C}_4\text{H}_9\text{N}^+\text{Me}_3)$	Si2(Q^4)	1 Si-O-Si		2x2x1	-2.2, -3.6 ^b	-2.5
$(\text{BSi}_{31}\text{O}_{70})^{13-} \cdot 13(\text{C}_4\text{H}_9\text{N}^+\text{Me}_3)$	Si2(Q^4)	2 Si-O-Si		2x2x1	-4.0	-1.9
$(\text{BSi}_{31}\text{O}_{70}\text{H}_{12})^- \cdot (\text{C}_4\text{H}_9\text{N}^+\text{Me}_3)$	Si2(Q^4)	2 Si-O-Si	12 SiOH	2x2x1	-3.4	-1.9

^a The ^{11}B experimental shift corresponds to the position of the experimental peak that gives the best match between all available experimental and calculation constraints.

^b depending on the position of the additional Si-O-Si connectivity.

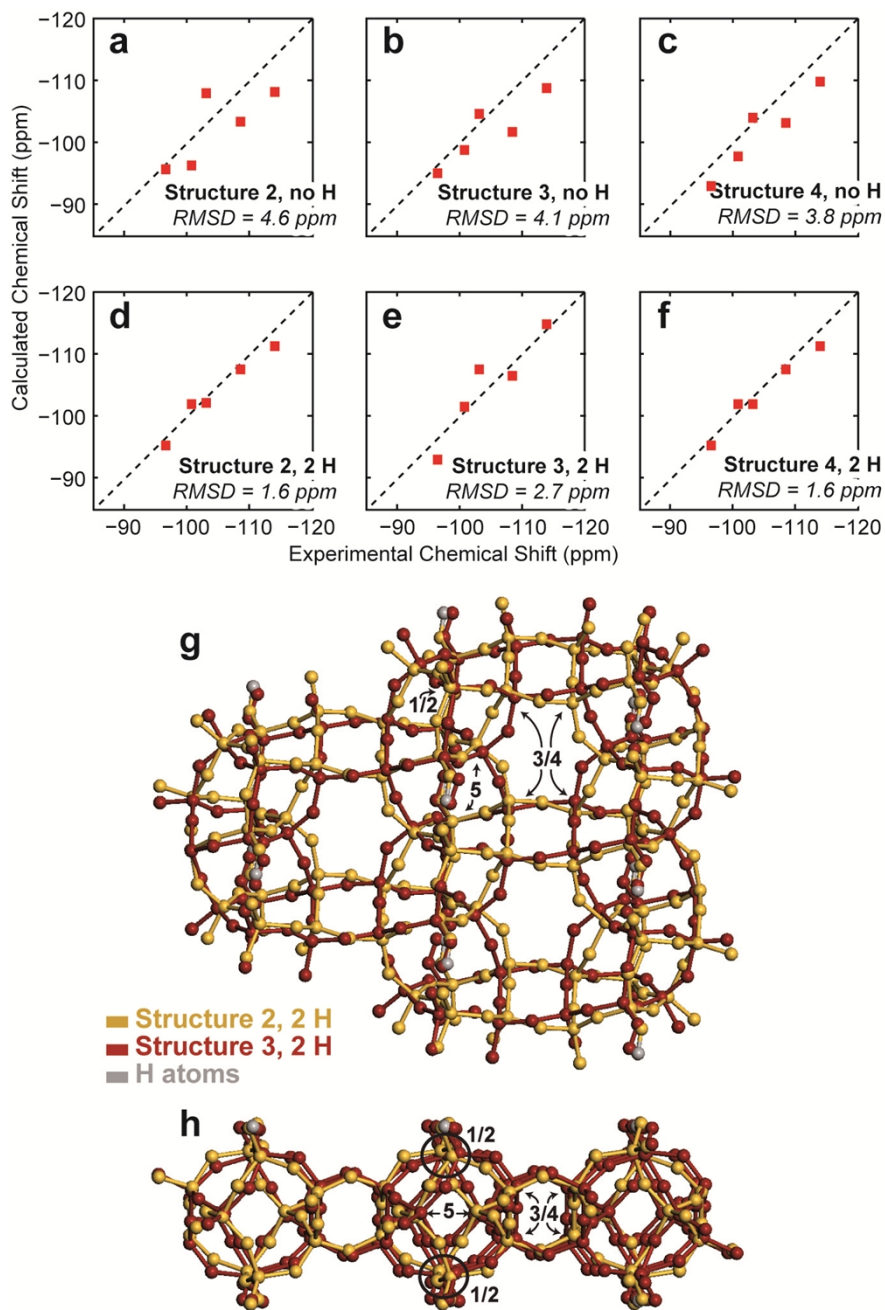


Figure S5. (a-f) Comparisons between experimental and calculated chemical shifts for candidate model structures of the reference $C_{16}H_{33}N^+Me_2Et$ -directed silicate material (without B incorporation). All structures optimized of the original structures labeled 2, 3 and 4 reported in ref. 2, with (a-c) no or (d-f) only 2 protons compensating the negative charges associated with non-bridging O atoms per supercell (consisting of 10 Si atoms and 22 O atoms). In contrast, the original structures published in ref. 2 had 4 H atoms per unit cell (data not shown here). Other negative charges are compensated here by positive charges homogeneously distributed across the

entire supercell. Best agreement between calculated and experimental ^{29}Si chemical shifts are obtained for the structures with 2 H per cell, which are superimposed and viewed from the top and from the side of the layer in (g) and (h). Structure 4 turns out to be identical to structure 2 when optimized under such conditions, and is consequently not shown.

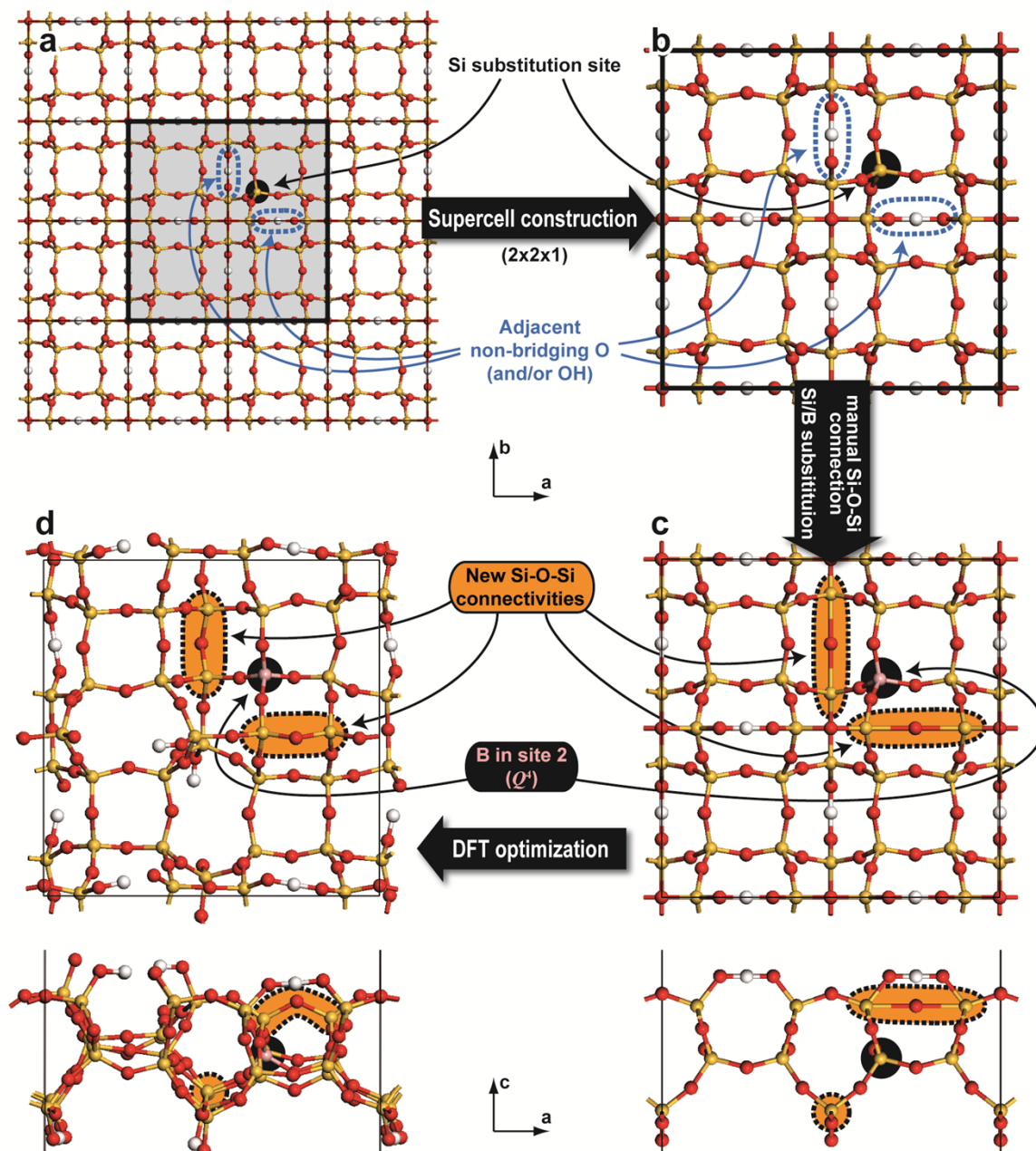


Figure S6. Illustration describing the procedure used to construct models of the $C_{16}H_{33}Me_3N^+$ -directed borosilicate material with two new Si-O-Si connectivities involving tetrahedral neighbors of a B atom incorporated in substitution of a Q^4 Si site. This situation can explain the unexpected absence of incompletely condensed $Q^3(1B)$ Si sites among the four connected tetrahedral neighbors of boron site B2. The DFT-optimized model at the bottom was obtained by replacing manually two pairs of nearby non-bridging O atoms in a $2 \times 2 \times 1$ supercell of the original model by a single O atom located at the center of mass of the corresponding Si atoms.

Table S4. Description of pseudopotentials used for plane-wave-based DFT calculations.

Atom	Core-states	Local channel	r_{loc} (a.u.)	r_{nonloc} (a.u.)	r_{aug} (a.u.)	Pseudopotential projectors	PAW projectors
H		p	0.8	0.8	0.6	2x2s	2x2s
B	1s	d	1.4	1.4	1.0	2x2s, 2x2p	2x2s, 2x2p
C	1s	d	1.4	1.4	1.0	2x2s, 2x2p	2x2s, 2x2p
N	1s	d	1.5	1.5	1.0	2x2s, 2x2p	2x2s, 2x2p
O	1s	d	1.3	1.3	0.9	2x2s, 2x2p	2x2s, 2x2p
Si	1s, 2s, 2p	d	1.8	1.8	1.3	2x3s, 2x3p	2x3s, 2x3p, 2x3d
Pseudopotentials used for calculations on reference crystalline systems (see below)							
Li		p	1.2	1.2	0.8	1x1s, 2x2s	1x1s, 2x2s
Na	1s	d	1.3	1.3	1.0	1x2s, 2x2p, 1x3s	1x2s, 2x2p, 1x3s
Mg	1s, 2s	d	1.6	2.0	1.4	2x3s, 1x2p, 2x3p	2x3s, 1x2p, 2x3p, 2x3d
Al	1s, 2s, 2p	d	2.0	2.0	1.4	2x3s, 2x3p	2x3s, 2x3p, 2x3d
P	1s, 2s, 2p	d	1.8	1.8	1.3	2x3s, 2x3p	2x3s, 2x3p, 2x3d
Ca	1s	f	1.6	2.0	1.4	1x3s, 2x3p, 1x4s	1x3s, 2x3p, 1x4s

Where r_{loc} is the pseudisation radius for the local component of the pseudopotential, r_{nonloc} is the pseudisation radius for the non-local components of the pseudopotential, and r_{aug} is the pseudisation radius for the charge augmentation functions. The corresponding Materials Studio castep on-the-fly strings used to generate these potentials are:

```
H 1|0.8|3.675|7.35|11.025|10UU(qc=6.4) []
Li 1|1.2|11|13.2|15|10U:20UU(qc=5.5) []
B 2|1.4|9.187|11.025|13.965|20UU:21UU(qc=5.5) []
C 2|1.4|9.187|11.025|12.862|20UU:21UU(qc=6) []
N 2|1.5|11.025|12.862|14.7|20UU:21UU(qc=6) []
O 2|1.3|16.537|18.375|20.212|20UU:21UU(qc=7.5) []
Na 2|1.3|1.3|1|11.8|13.6|15.3|20U=-2.07:30U=-0.105:21U=-1.06U=+0.25 []
Mg 2|1.6|2|1.4|6|7|8|30NH:21U:31UU:32LGG(qc=4.5) []
Al 2|2|3.675|5.512|7.717|30UU:31UU:32LGG []
Si 2|1.8|3.675|5.512|7.35|30UU:31UU:32LGG []
P 2|1.8|3.675|5.512|6.982|30UU:31UU:32LGG []
Ca 3|1.6|2.0|1.4|7|9|10|30U:40U:31:32U=+0@+0.12U=+1.0@+0.12
```

The pseudopotential of Ca used the correction described by Profeta *et al.*⁵

Table S5. Calculated shielding (σ_{iso}) and experimental chemical shifts (δ_{iso}) of reference systems of known crystal structure.

Nucleus	Compound, formula	Site #	Experimental shift (ppm)	Reference	Calculated shielding (ppm)	
²⁹ Si	α -quartz SiO ₂	1	-107.4	6	429.6	
	Cristoballite SiO ₂	1	-108.5	6	430.9	
	albite NaAlSi ₃ O ₈		3	-105		428.0
			2	-97	7	419.0
			1	-93		414.4
	datolite CaBSiO ₄ (OH)	1	-83	6	404.4	
	danburite CaB ₂ Si ₂ O ₈	1	-89	6	410.1	
	Pyrophyllite Si ₄ Al ₂ O ₁₀ (OH) ₂	1	-94	7	416.7	
	Talc Si ₄ Mg ₃ O ₁₀ (OH) ₂	1	-97	7	420.0	
	Na ₂ SiO ₃	1	-76.8	6	396.9	
	α -Na ₂ Si ₂ O ₅	1	-93.6	8	416.5	
	β -Na ₂ Si ₂ O ₅		1	-85.6		406.5
			2	-87.5	8	408.0
	δ -Na ₂ Si ₂ O ₅		1	-90.6		411.7
			2	-90.2	9	411.2
¹¹ B	Reedmegnerite NaBSi ₃ O ₈	1	-1.9	7	96.31	
	Datolite CaBSiO ₄ (OH)	1	1.0	7	93.38	
	Danburite CaB ₂ Si ₂ O ₈	1	0.7	7	95.45	
	BN cubic	1	1.6	7	94.80	
	BN hexagonal	1	30.4	7	66.40	
	diomignite Li ₂ B ₂ O ₇	1	17.9		76.22	
	dilithium tetraborate	2	1.7	7	92.04	
	BPO ₄	1	-3.3	7	98.23	
	Sassolite B(OH) ₃	1	18.8	7	74.70	

Calculations of shieldings for crystalline model systems of known structure and experimental shifts are used to accurately calculate the isotropic ²⁹Si and ¹¹B chemical shifts (δ_{iso}) from calculated ²⁹Si and ¹¹B shieldings (σ_{iso}). This procedure compensates for possible systematic errors of the DFT calculations. All calculations were conducted on structures previously optimized with fixed unit cell parameters. The series of compounds listed in Table S3 led to the following relationships: $\delta_{\text{iso}}(\text{ppm}) = -0.920 \cdot \sigma_{\text{iso}} + 288.45$ for ²⁹Si ; and $\delta_{\text{iso}}(\text{ppm}) = -1.0 \cdot \sigma_{\text{iso}} + 95.3$ for ¹¹B.

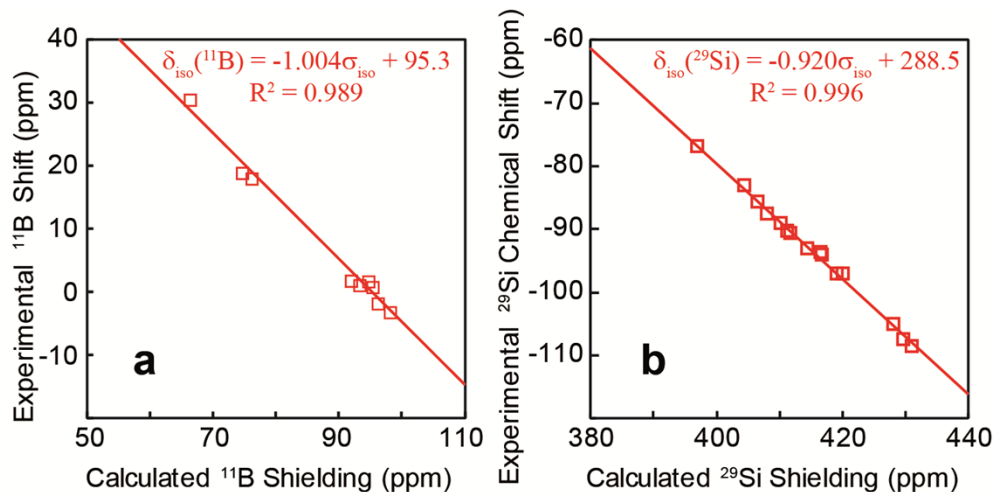


Figure S7. Correlation plots between experimental isotropic chemical shifts and isotropic shielding calculated by DFT for the series of reference crystals of known structures listed in Table S3. The figures (a) and (b) correspond to ^{11}B and ^{29}Si NMR data, respectively.

References of the Supporting Information section.

1. I. Wolf, H. Gies and C. A. Fyfe, *The Journal of Physical Chemistry B*, 1999, **103**, 5933-5938.
2. D. H. Brouwer, S. Cadars, J. Eckert, Z. Liu, O. Terasaki and B. F. Chmelka, *J. Am. Chem. Soc.*, 2013.
3. S. Cadars, N. Mifsud, A. Lesage, J. D. Epping, N. Hedin, B. F. Chmelka and L. Emsley, *J. Phys. Chem. C*, 2008, **112**, 9145–9154.
4. D. H. Brouwer, S. Cadars, J. Eckert, Z. Liu, O. Terasaki and B. F. Chmelka, *J. Am. Chem. Soc.*, 2013, **135**, 5641-5655.
5. M. Profeta, M. Benoit, F. Mauri and C. J. Pickard, *J. Am. Chem. Soc.*, 2004, **126**, 12628-12635.
6. J. F. Stebbins, in *Handbook of Physical Constants*, ed. T. J. Ahrens, American Geophysical Union, Washington D.C., 1995, vol. 2.
7. K. J. D. Mackenzie and M. E. Smith, *multinuclear solid-state NMR of inorganic materials*, Pergamon Press, Oxford, 2002.
8. H. Koller, G. Engelhardt, A. P. M. Kentgens and J. Sauer, *J. Phys. Chem.*, 1994, **98**, 1544-1551.
9. L. Martel, S. Cadars, E. Véron, D. Massiot and M. Deschamps, *Solid State Nucl. Mag.*, 2012, **45–46**, 1-10.